

Effects of the Cu Ion on the Structural and Optical Properties of Yttrium Doped ZnO by Solution Combustion

S. López-Romero, M. J. Quiroz-Jiménez, M. García-Hipólito, A. Aguilar-Castillo

Departamento de Materia Condensada y Criogenia, Universidad Nacional Autónoma de México, Instituto de Investigaciones en Materiales, circuito exterior S/N Ciudad de México Coyoacán, Ciudad de México, México

Email: sebas@unam.mx

How to cite this paper: López-Romero, S., Quiroz-Jiménez, M.J., García-Hipólito, M. and Aguilar-Castillo, A. (2017) Effects of the Cu Ion on the Structural and Optical Properties of Yttrium Doped ZnO by Solution Combustion. *World Journal of Condensed Matter Physics*, 7, 89-98.

<https://doi.org/10.4236/wjcmp.2017.74008>

Received: August 5, 2017

Accepted: October 30, 2017

Published: November 2, 2017

Copyright © 2017 by authors and Scientific Research Publishing Inc.

This work is licensed under the Creative Commons Attribution-NonCommercial International License (CC BY-NC 4.0).

<http://creativecommons.org/licenses/by-nc/4.0/>



Open Access

Abstract

In this experiment, pure, Y^{3+} doped ZnO and $Cu^{2+} + Y^{3+}$ co-doped ZnO were synthesized by a solution combustion method. The Y^{3+} dopant concentration was fixed in 3%wt. and the Cu^{2+} dopant concentrations were 0, 1, 2, 3, 10, and 20%wt. The XRD spectra showed that the original hexagonal wurtzite structure of ZnO is conserved after doping process, an increasing red shift until 10%wt. Cu^{2+} doping and decrease at higher Cu^{2+} doping and also, the chemical creation of the new Y_2O_3 and $Y_2Cu_2O_5$ phases. The behavior of the photoluminescence of the samples as a function of Cu^{2+} doping reveal that the green emission band of the ZnO is quenching and the ZnO UV emission intensity decrease notably for all Cu^{2+} doping. The scanning electron microscope analysis of the $Cu^{2+} + Y^{3+}$ co-doped ZnO samples reveal the existence of grains agglutinated forming like-spheres particles. However, the nano-sized characteristic of the crystals is confirmed.

Keywords

Zinc Oxide, Solution Combustion, X-Ray, Photoluminescence, Morphology

1. Introduction

The zinc oxide (ZnO) is one of the oldest n-type semiconductor material studied, and is actually a promising material in fundamental studies and technological applications due to its varied and outstanding properties such as: high conductance and transparency in thin films, chemical and thermal stability, wide band gap (3.37 eV) and a large exciton binding energy (60 meV) [1], which presents efficient photoluminescence and thermo-luminescence in intrinsic state

[2]. The property that has the ZnO of can be doped opened a lot of technological applications: doping of ZnO for fabricating semiconductor devices such as vacuum fluorescent displays, field emission displays [3], solar cells [4], magnetic [5], photoluminescent [6], electro-optical [7], etc. The ZnO can be synthesized by various methods, such as electrodeposition [8], evaporation [9], vapor-liquid-solid (VLS) growth [10], metal-organic catalyst, assisted vapor-phase epitaxy [11], aqueous thermal decomposition [12], microwave activated chemical bath deposition (MW-CBD) [13], chemical bath deposition (CBD) [14], surfactant-assisted hydrothermal method [15], and solution combustion method [16] [17]. This last method is more convenient than other because it is pensive, it has an easier composition control, and coating can be deposited on large area etc. Co-doping of host matrix is a technique for incorporating two or more elements into a host lattice with the objective of change sum or improves the properties physical and chemical of the host matrix. The ZnO has been co-doped with various elements (rare earth, lanthanides, metals, etc.) combined [2] [3] [4], in special with Cu^{2+} ions to tailoring the optical properties of Y^{3+} doped ZnO compounds because the Cu^{2+} ion has the capacity of: modify the luminescence of ZnO crystals by creating localized impurity levels [9] [18]. But also the Cu^{2+} ion can quench some emission photoluminescence type [19] as will be showed in this study. However, the doping of ZnO with Cu^{2+} ions cannot modify ZnO structure [20]. In turn, the Y^{3+} element belong to rare earth periodic family [5] [6], the importance of Y^{3+} is its capacity for tailoring the optical properties of ZnO, because Y^{3+} doping decrease the energy band gap of ZnO [7]. The Y^{3+} surface hinders crystalline growth and promotes vacancies generation [21]. In this experiment, the possible effects caused by the Cu^{2+} ions on the structural and optical properties of Y^{3+} doped ZnO compounds are analyzed and explicated. The $\text{Cu}^{2+} + \text{Y}^{3+}$ co-doping process is realized by a solution combustion technique.

2. Experimental Details

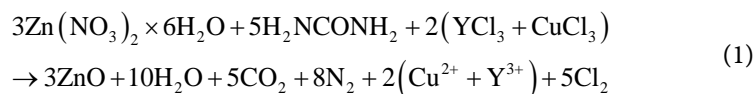
2.1. The Solution Combustion Method

The experimental method of chemical synthesis solution combustion [17], is quite simple, fast and economical in which an oxidizer and a fuel agents are combined in a highly exothermic red-ox chemical reaction stoichiometric, producing ZnO, H_2O (vapor), molecular N_2 , and CO_2 . In this work using Zinc Nitrate hexahydrate [$\text{Zn}(\text{NO}_3)_2 \cdot 6\text{H}_2\text{O}$] as oxidizer, urea [$(\text{H}_2\text{NCONH}_2)$] as fuel, yttrium chloride [YCl_3] and copper chloride [CuCl_2] as dopants, undoped and $\text{Cu}^{2+} + \text{Y}^{3+}$ doped ZnO were synthesized by a solution combustion technique as a function of Cu^{2+} ion concentration in %wt, maintaining the Y^{3+} concentration constant in 3%wt. The samples were later annealed at 835°C by 2 h.

2.2. Stoichiometric Equation

Pure and $\text{Cu}^{2+} + \text{Y}^{3+}$ doped ZnO samples were obtained by a solution combustion technique by means of the following redox chemical reaction stoichiome-

tric:



The Equation (1) was obtained by taken into account the oxidizer/fuel molar ratio ($O/F = 1$) required for a stoichiometric mixture which is determined by summing the total oxidizing and reducing valences in the oxidizer compound and dividing it by the sum of the total oxidizing and reducing valences in the fuel compound [17]. Accordingly for the complete combustion of zinc nitrate-urea mixture, the molar ratio becomes 5/3, the equation balanced (1) was obtained with this value ratio. Using the weight atomic concept in Equation (1), it was used to obtain 3 gr. of ZnO for all the Cu^{2+} ion concentrations. The dopants yttrium and copper by means its respective chloride were simultaneously integrated into ZnO host in each combustion reaction using the dopants concentrations correct. The samples produced were characterized by x-ray diffraction technique using a Philips PW 1800 diffractometer using Cu $K\alpha$ radiation, the morphology of the samples was studied by means of a scanning electron microscopy JEOL JSM 840 A, and the photoluminescence spectra was recorded using a Tektronix 792 AD.

3. Results and Discussion

3.1. X-Ray Diffraction (XRD) Study

The XRD patterns of Y^{3+} doped ZnO with 3%wt. and $\text{Cu}^{2+} + \text{Y}^{3+}$ co-doped ZnO with 3%wt. of Y^{3+} ion and 1, 3, 5, 10, and 20%wt. of Cu^{2+} ion concentrations and after annealed at 835°C by 2 h are showed in **Figure 1**. The observed XRD characteristic peaks positioned in 2θ scale at 31.64 , (100), 34.32 , (002), 36.02 , (101), 47 , 45 , (102), 56.49 , (110), 62.70 , (103), 66.30 , (201), 67.85 , (112) and 69.93 , (201) shows the good crystallinity of the material. All the diffraction peaks can be indexed to the hexagonal wurtzite structure of ZnO (JCPDS card No. 36-1451, $a = b = 3.249\text{Å}$, $c = 5.206\text{Å}$). However, other characteristic peaks at 29° , (222) and 27° , (230), corresponding to the yttrium oxide (Y_2O_3) and $\text{Y}_2\text{Cu}_2\text{O}_5$ phases respectively also were observed in $\text{Cu}^{2+} + \text{Y}^{3+}$ co-doped ZnO, which can be attributed to the doping of Y^{3+} ion into Zn^{2+} lattice site. Also, it is observed that the peak intensity of the news phases decrease with Cu^{2+} ion concentration until total quenching at 20%wt. due to Cu^{2+} ion incorporation into Zn-Y-O lattice site and segregation of Y^{3+} ion toward ZnO surface. The $\text{Y}_2\text{Cu}_2\text{O}_5$ phase also is obtained as secondary phase in the YBaCuO superconductor synthesis [22] [23] [24] [25]. The **Figure 2** shows a magnification of the (002) plane between 34.1° and 34.7° in which are observed the changes in peak intensity and peak position as a function of Cu^{2+} ion concentration. The peak intensity is increased when the Cu^{2+} ion is incorporated into Y^{3+} -Zn-O lattice until 10%wt. Cu^{2+} ion concentration. This is attributed to the Cu^{2+} interstitial existence sharing the

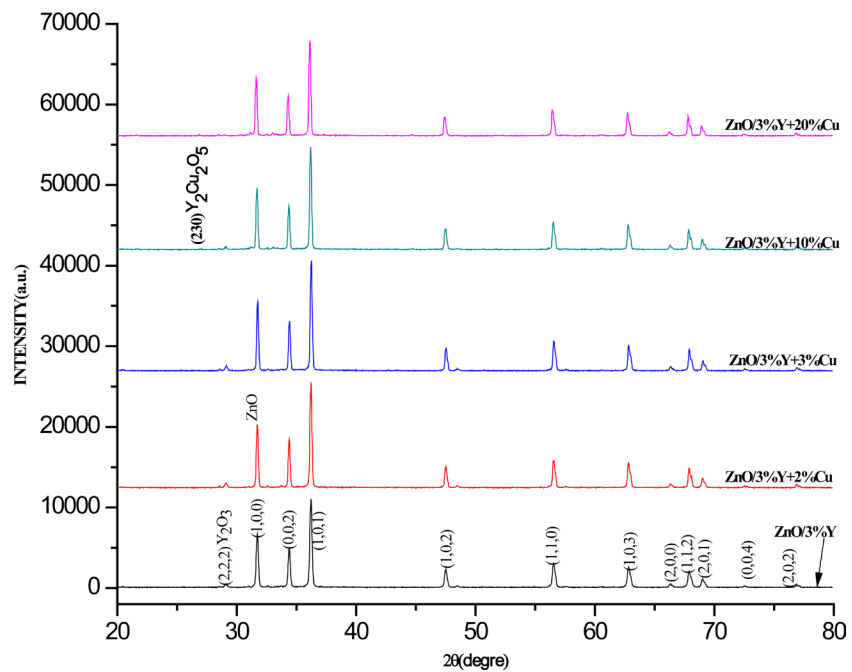


Figure 1. XRD patterns of Y^{3+} doped (3%wt.) ZnO and $Cu^{2+} + Y^{3+}$ co-doped ZnO as a function of Cu^{2+} ion concentration in %wt.

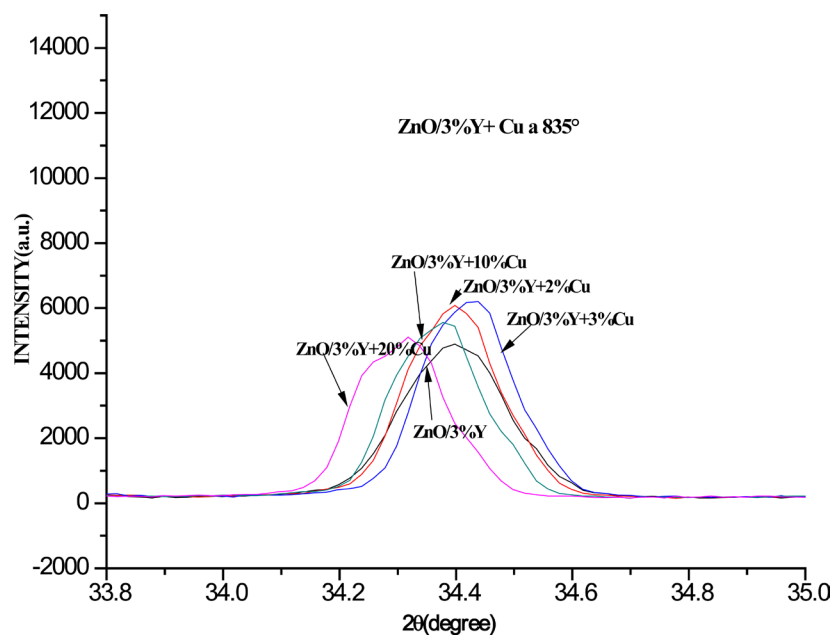


Figure 2. Red shift of the (002) enlarged plane as a function of Cu^{2+} ion concentration in %wt.

oxygen with the Zn^{2+} atoms increasing the peak intensity. After 10%wt. the peak intensity decrease, due to excess of Cu^{2+} atoms that are energetically efficient to coalesce into metallic copper cluster decreasing the peak intensity [20]. The peak position along (002) plane of $Cu^{2+} + Y^{3+}$ co-doped ZnO samples is red shifted in 2θ scale and broader up to 10%wt. Cu^{2+} ion concentration, after this value the peak position is increased newly due to the effect by intercalation of Cu^{2+} ion on

the interatomic distance of the Y-Zn-O lattice [20]. The average crystal size of the samples was obtained from diffraction (101) plane using the Debye-Scherrer equation:

$$D = \frac{0.9\lambda}{\beta \cos \theta} \quad (2)$$

where λ is the X-ray wavelength used (1.5406Å), β is the full width at half maximum (FWHM) along (101) plane and theta is the Bragg diffraction angle. The **Figure 3(a)** and **Figure 3(b)** shows the change in FWHHM and average crystal

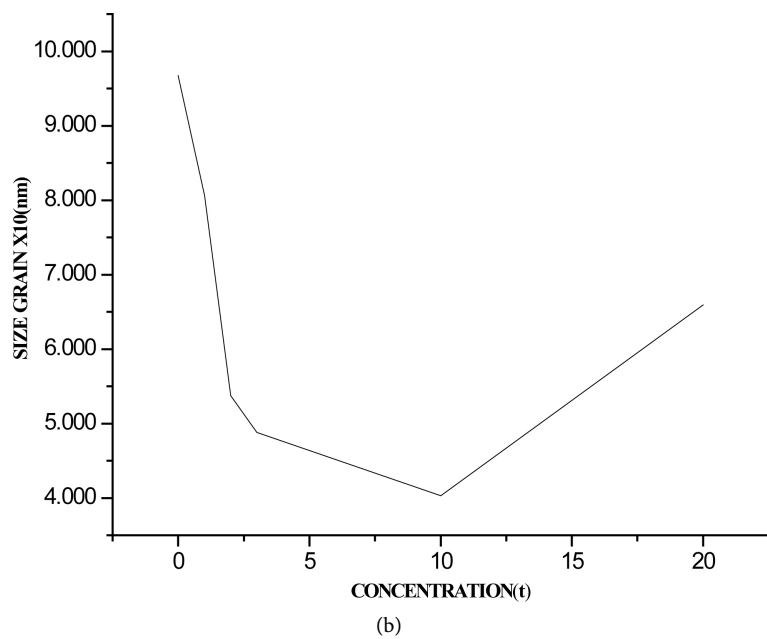
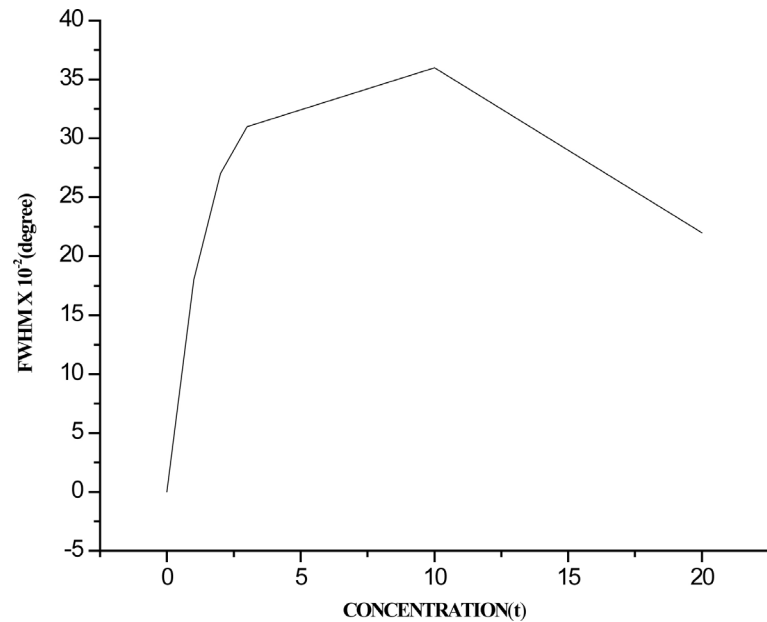


Figure 3. (a) FWHM; (b) average crystal size, as a function of Cu^{2+} ion concentration in %wt.

size as a function of Cu^{2+} ion concentration respectively, it is observed from **Figure 3(a)** that the FWHM increases with Cu^{2+} ion concentration until reach a maximum value at 10 %wt., after this value decrease until reach a value minimum. In contrary, from **Figure 3(b)** it is observed that the crystal size decrease with the Cu^{2+} ion concentration until reach a minimum value in 10%wt. after this value the crystal size increase. This behavior between the FWHM and the average crystal size is predicted by the Debye-Scherrer equation, since for a maximum value of FWHM correspond a minimum value in crystal size. Also it is observed that the $\text{Cu}^{2+} + \text{Y}^{3+}$ co-doped ZnO crystals have less size than Y^{3+} doped ZnO; the initial reduction size from 75 nm with 0.0%wt. of Cu^{2+} ion to 40 nm whit 10%wt. of Cu^{2+} ion is due to the distortion produced by Cu^{2+} ions intercalated in the Zn-Y-O lattice [20]. At higher Cu^{2+} concentration than 10%wt. the Cu^{2+} atoms excess is combined forming the $\text{Y}_2\text{Cu}_2\text{O}_5$ compound.

3.2. Photoluminescence Study

The **Figure 4** shows the photoluminescence (PL) spectra of pure ZnO and Y^{3+} doped ZnO with 3%wt. The spectra were obtained in the UV-Vis range, illuminated with an excitation wavelength of 350 nm at room temperature. The PL spectrum of pure ZnO samples, exhibits the typical main band with characteristics peaks centered about 390 nm and corresponds to the near band edge (NBE) emission [6]. At higher wavelengths than NBE diffraction peak appears with less intensity that NBE peak the green emission band centered about 518 nm and attributed to free exciton recombination. From **Figure 4** can be observed and calculated a little blue shift when Y^{3+} dopant was incorporated into ZnO host lattice, changing the ultra-violet NBE emission from 390 to 382 nm increasing the ZnO band gap in 0.3 eV. This slight blue shift of the UV peak is caused by 3%wt. Y^{3+} doping [9] and [16]. However it is observed an increase in UV intensity in Y^{3+} doped ZnO compared with UV intensity of pure ZnO. The **Figure 5** exhibit the room temperature PL spectra of $\text{Cu}^{2+} + \text{Y}^{3+}$ co-doped ZnO samples with var-

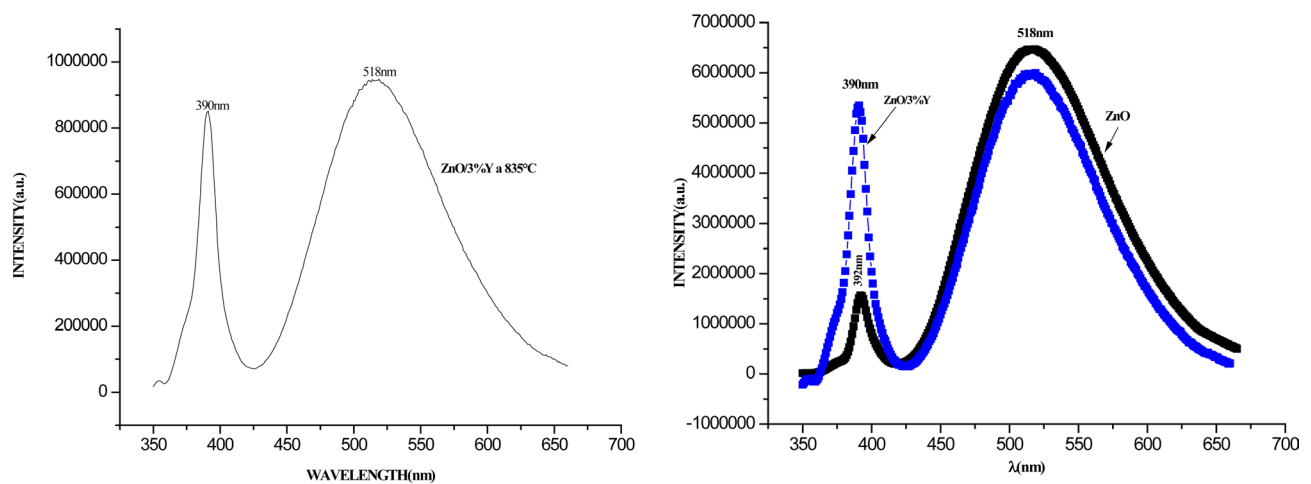


Figure 4. Photoluminescence spectrum of pure ZnO and doped ZnO with 3%wt. Y^{3+} ion. The samples were illuminated using a wavelength excitation of 350 nm.

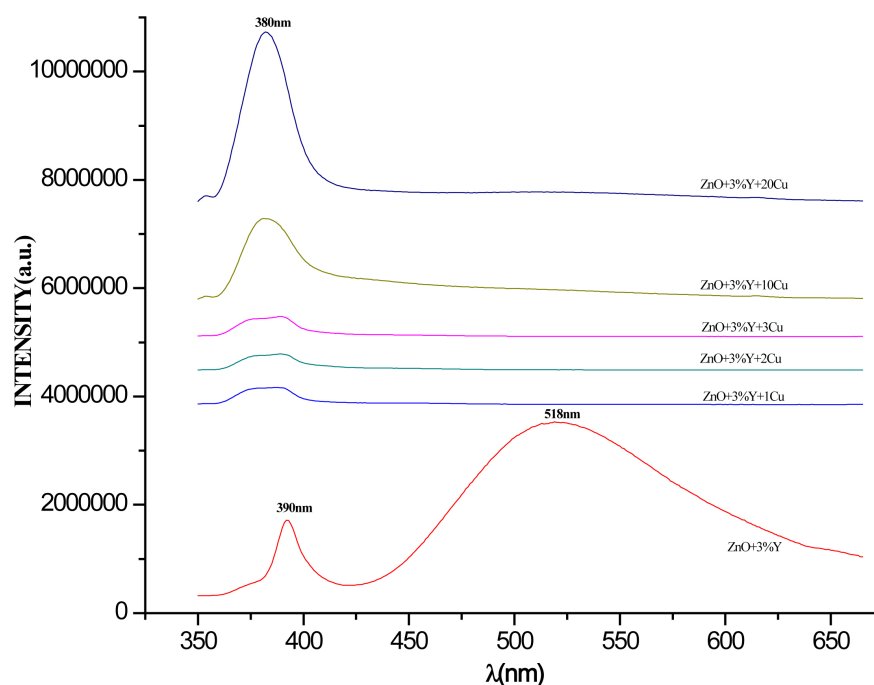


Figure 5. Photoluminescence spectra of $\text{Cu}^{2+} + \text{Y}^{3+}$ co-doped ZnO as a function of Cu^{2+} ion concentration in %wt.

ious Cu^{2+} ion concentrations values of 2, 3, 5, 10 and 20%wt., it is clearly observed that for all Cu^{2+} concentration the green PL emission due to free exciton recombination has been quenched by the intercalation of Cu^{2+} ions into $\text{Y}^{3+} + \text{ZnO}$ host lattice; this quenching effect is attributed to a non-radiative recombination process known as non-radiative recombination Auger phenomena which is associated to degenerate electrons, in which the energy released by an electron is immediately recombined and absorbed by another electron and the energy involved is dissipated by phonons. Auger process is considered as the cause major of non-radiative recombination in semiconductor materials. Auger process depends on the doping atoms concentration and defects in the lattice. [19]. However, in Fig. 5 also it is observed that the UV-NBE emission of the samples is diminished by increasing Cu^{2+} ion concentration, indicating that the optical-gap of ZnO semiconductor can be tailored by means of Cu^{2+} doping. This last result can be technologically applied in UV radiation sensors fabrication [26].

3.3. Morphology Study

The scanning electron microscope (SEM) technique has been used to observe the surface morphology (SM) of the particles. The **Figures 6(a)-(d)** exhibits the SEM images of the SM of $\text{Cu}^{2+} + \text{Y}^{3+}$ co-doped ZnO. The **Figure 6(a)** shows the SM of Y^{3+} doped ZnO sample, it presents the existence of like-ovoid particles compact, dense structure and forming layers which have its surface covered with grains of size similar that are unevenly distributed. The average size grain is of 30 nm. The **Figure 6(b)** shows the SM of $\text{Cu}^{2+} + \text{Y}^{3+}$ co-doped ZnO with 2%wt. of Cu^{2+} ions concentration, it is observed that the grains are most agglomerated

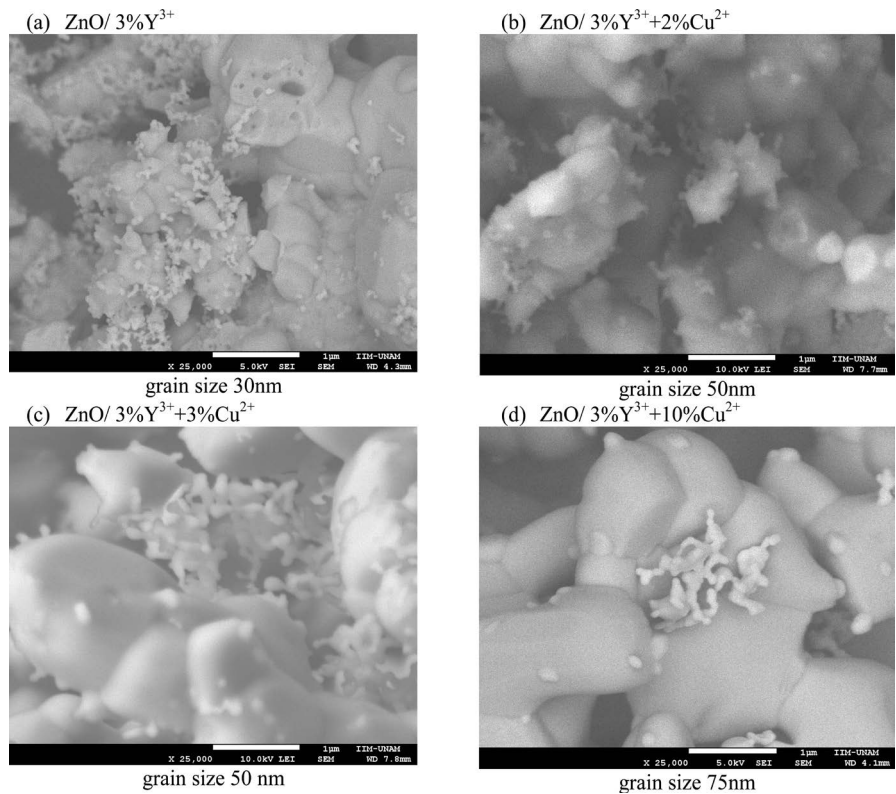


Figure 6. Surface morphology of $\text{Cu}^{2+} + \text{Y}^{3+}$ doped ZnO as a function of Cu^{2+} ion concentration in %wt. and 3% of Y^{3+} fixed.

and evenly distributed in the sample. In this case the grains have an average size of 50 nm. The **Figure 6(c)** exhibits the SM of the $\text{Cu}^{2+} + \text{Y}^{3+}$ co-doped ZnO with 3%wt. of Cu^{2+} ions concentration. It is seen that further increase in the intercalation of Cu^{2+} ions into Zn-Y-O host lattice improves the crystallinity of the sample. The **Figure 6(c)** displays the SM of $\text{Cu}^{2+} + \text{Y}^{3+}$ co-doped ZnO with 3%wt. of Cu^{2+} ions, the particles presents like-spheres form and higher size than Y^{3+} doped ZnO. The average grain size of these particles is 50 nm. Finally the **Figure 6(d)** exhibits the SM of $\text{Cu}^{2+} + \text{Y}^{3+}$ co-doped ZnO with 10%wt. of Cu^{2+} ions concentration. In this Cu^{2+} concentration level is observed the presence of the $\text{Y}_2\text{Cu}_2\text{O}_5$ as is corroborated by the XRD patterns showed in **Figure 1**. However, also can be seen Cu^{2+} ions interstitial localized into ZnO matrix. The geometry of these particles is like-spheres with an average size of 75 nm.

4. Conclusion

In this study, pure and $\text{Cu}^{2+} + \text{Y}^{3+}$ co-doped ZnO were synthesized as a function of Cu^{2+} ion concentration by a solution combustion method. The XRD study showed that the hexagonal wurtzite structure of ZnO is maintained after Cu^{2+} doping process. Using the (002) plane of XRD spectra, a red shift was observed due to Cu^{2+} doping process. The PL results for Y^{3+} doped ZnO showed a UV intensity higher compared with the UV intensity of pure ZnO. For all the Cu^{2+} ion concentrations, the green PL emission is quenching by Cu^{2+} doping effect. The

UV PL emission can be tailored by Cu²⁺ doping effect. In 10%wt. of Cu²⁺ doping, the Y₂Cu₂O₅ phase is created. A blue shift of 0.3 eV is observed in the UV PL emission of Cu²⁺ + Y³⁺ samples due to Cu²⁺ doping effect.

Acknowledgements

The authors wish to thank to Dr. Ciro Falcony (IPN), Adriana Tejada (IIM) for the XRD measurements, to Omar Novelo Peralta (IIM) for his SEM study, to M.A. Canseco Martinez (IIM) for their chemical analysis.

References

- [1] Tang, Z.K., Wong, G.K.L., Yu, P., Kawasaki, M., Ohtomo, A., Koinuma, H. and Segawa, Y. (1998) Room-Temperature Ultraviolet Laser Emission from Self-Assembled ZnO Microcrystallite Thin Films. *Applied Physics Letters*, **72**, 3270-3272. <https://doi.org/10.1063/1.121620>
- [2] Xu, H.Y., Liu, Y.C., Ma, J.G., Luo, Y.M., Lu, Y.M., Shen, D.Z., Zhang, J.Y., Fan, X.W. and Mu, R. (2004) Photoluminescence of F-Passivated ZnO Monocrystalline Films Made from Thermally Oxidized ZnF₂ Films. *Journal of Physics: Condensed Matter*, **16**.
- [3] Xu, H.Y., Liu, Y.C., Liu, Y.X., Xu, C.S., Shao, C.L. and Mu, R. (2006) Structural, optical, and Magnetic Properties of Mn-Doped ZnO Thin Film. *The Journal of Chemical Physics*, **124**, 074707. <https://doi.org/10.1063/1.2171308>
- [4] Zhang, Y.Q., Heng, L.P. and Jiang, L. (2014) Chemically Controllable Fabrication of One-Dimensional ZnO Nanostructures and Their Applications in Solar Cells Source. *Journal of Nanoscience and Nanotechnology*, **14**, 5597-5613. <https://doi.org/10.1166/jnn.2014.8862>
- [5] Gorla, C.R., Emanetoglu, N.W., Liang, S., Mayo, W.E., Lu, Y., Wraback, M. and Shen, H. (2000) Ultraviolet Detectors Based on Epitaxial ZnO Films Grown by MOCVD. *Journal of Electronic Materials*, **29**, 69-77. <https://doi.org/10.1007/s11664-000-0097-1>
- [6] Mendoza-Galván, A., Trejo-Cruz, C., Lee, J., Bhattacharyya, D. and Metson, J. (2006) Effect of Metal-Ion Doping on the Optical Properties of Nanocrystalline ZnO Thin Films. *Journal of Applied Physics*, **99**, 014306. <https://doi.org/10.1063/1.2158503>
- [7] Xu, H.Y., Liu, Y.C., Mu, R., Shao, C.L., Lu, Y.M., Shen, D.Z. and Fan, X.W. (2005) Room-Temperature Ferromagnetism in (Mn, N)-Codoped ZnO Thin Films Prepared by Reactive Magnetron Cosputtering. *Applied Physics Letters*, **88**, 242502. <https://doi.org/10.1063/1.2213929>
- [8] Garcia, P.F., McLean, R.S., Reilly, M.H. and Nunes, G. (2003) Transparent ZnO Thin-Film Transistor Fabricated by RF Magnetron Sputtering. *Applied Physics Letters*, **82**, 1117-1119. <https://doi.org/10.1063/1.1553997>
- [9] Umar, A., Karunakaran, B., Suh, E.-K. and Hahn, Y.B. (2006) Structural and Optical Properties of Single-Crystalline ZnO Nanorods Grown on Silicon by Thermal Evaporation. *Nanotechnology*, **17**, 4072-4077. <https://doi.org/10.1088/0957-4484/17/16/013>
- [10] Zhao, Q.X., Klason, P. and Willander, M. (2007) Growth of ZnO Nanostructures by Vapor-Liquid-Solid Method. *Applied Physics A*, **88**, 27-30. <https://doi.org/10.1007/s00339-007-3958-0>

- [11] Lee, C.-H. and Yi, G.-C. (2011) Catalyst-Free Metal-Organic Vapor-Phase Epitaxy of ZnO and GaN Nanostructures for Visible Light-Emitting Devices. *NanoScience and Technology*. Springer, Heidelberg, Dordrecht, London, New York.
- [12] Su, X., Zhang, Z., Wang, Y. and Zhu, M. (2005) Synthesis and Photoluminescence of Aligned ZnO Nanorods by Thermal Decomposition of Zinc Acetate at a Substrate Temperature of $\sim 250^\circ\text{C}$. *Journal of Physics D: Applied Physics*, **38**, 3934-3937. <https://doi.org/10.1088/0022-3727/38/21/015>
- [13] Díaz-Reyes, J., Martínez-Juárez, J., García, M.L., Juárez, G. and Galeazzi, R. (2010) Growth and Characterization of ZnO Films Deposited by Chemical Bath and Annealed by Microwaves (CBD-A μ W). *Materials Science and Engineering*, **12**, Article ID: 012003.
- [14] Nkrumah, I., Ampong, F.K., Kwakye-Awuah, B., Nkum, R.K. and Boakye, F. (2013) Synthesis and Characterization of ZnO Thin Films Deposited by Chemical Bath Technique. *IJRET*, Vol. 2.
- [15] López-Romero, S. and García-H, M. (2013) Photoluminescence and Structural Properties of ZnO Nanorods Growth by Assisted-Hydrothermal Method. *World Journal of Condensed Matter Physics*, **3**, 152-157.
- [16] Tonio, J.C., Takimi, A.S. and Bergmann, C.P. (2010) Nanostructured Cobalt Oxides (Co₃O₄ and CoO) and Metallic Co Powders Synthesized by the Solution Combustion Method. *Materials Research Bulletin*, **45**, 672-676.
- [17] Patil, K.C. and Hegde, M.S. (2008) Chemistry of Nanocrystalline Oxide Materials. World Scientific Publishing Co. Pte. Ltd., 42-59.
- [18] Tao, Y.M., Ma, S.Y., Chen, H.X., Meng, J.X., Hou, L.L., Jia, Y.F. and Shang, X.R. (2011) Effect of the Oxygen Partial Pressure on the Microstructure and Optical Properties of ZnO: Cu Films. *Vacuum*, **85**, 744-748.
- [19] López-Romero, S., Quiroz-Jiménez, M.J. and García-Hipólito, M. (2016) Quenching Photoluminescence of Eu(III) by Cu(II) in ZnO:Eu³⁺:Cu²⁺ Compounds by Solution Combustion Method. *World Journal of Condensed Matter Physics*, **6**, 269-275. <https://doi.org/10.4236/wjcmp.2016.63025>
- [20] Anandan, S. and Muthukumaran, S. (2014) Structural and Optical Properties of Y, Cu doped ZnO Nanoparticles by Sol-Gel Method. *Superlattices and Microstructures*, **74**, 247-260.
- [21] Sanoopa, P.K., Anasa, S., Ananthakumara, S., Gunasekarb, V., Saravananb, R. and Ponnusamib, V. (2016) Synthesis of Yttrium Doped Nanocrystalline ZnO and Its Photocatalytic Activity in Methylene Blue Degradation. *Arabian Journal of chemistry*, **9**, S1618-S1626. <https://doi.org/10.1016/j.arabjc.2012.04.023>
- [22] Ramakrishna, B.L. and Ong, E.W. (1988) Magnetic Properties of Y₂Cu₂O₅. *Solid State Communications*, **68**, 775-779.
- [23] García-Muñoz, J.L. and Rodríguez-Carvajal, J. (1990) Ferromagnetic Layers in Y₂Cu₂O₅: A Neutron Diffraction Study. *Kidlington, Royaume-Uni*, **149**, 319-327.
- [24] Matsuok, Y., Nishimura, Y., Mitsudo, S. and Nojiri, H. (1998) Metamagnetic Transition in Y₂Cu₂O₅. *Journal of Magnetism and Magnetic Materials*, **177-181**, 729-730.
- [25] Famery, R. and Queyroux, F. (1989) Crystal Structure Refinement Y₂Cu₂O₅ from Single Crystal X-Ray Diffraction Data. *Materials Research Bulletin*, **24**, 275-285.
- [26] Yu, Q., Fu, W., Yu, C., Yang, H., Wei, R., Sui, Y., Liu, S., Liu, Z., Li, M. and Wang, G. (2007) Structural, Electrical and Optical Properties of Yttrium-Doped ZnO Thin Films Prepared by Sol-Gel Method. *Journal of Physics D: Applied Physics*, **40**, 5592-5597.